*buildings*

MDPI

*Article*

# Hybrid Machine Learning Algorithms for Prediction of Failure Modes and Punching Resistance in Slab-Column Connections with Shear Reinforcement

**Huajun Yan [1,*], Nan Xie [1] and Dandan Shen [2]**

[1] School of Civil Engineering, Beijing Jiaotong University, Beijing 100044, China; n_xie@sina.com
[2] SANY Heavy Industry Co., Ltd., Beijing 100044, China; shendd2@sany.com.cn
* Correspondence: 19115044@bjtu.edu.cn

**Abstract:** This study presents a data-driven model for identifying failure modes (FMs) and predicting the corresponding punching shear resistance of slab-column connections with shear reinforcement. An experimental database that contains 328 test results is used to determine nine input variables based on the punching shear mechanism. A comparison is conducted between three typical machine learning (ML) approaches: random forest (RF), light gradient boosting machine (LightGBM), extreme gradient boosting (XGBoost) and two hybrid optimized algorithms: grey wolf optimization (GWO) and whale optimization algorithm (WOA). It was found that the XGBoost classifier had the highest accuracy rate, precision, and recall values for FM identification. In testing, WOA-XGBoost has the best accuracy in predicting punching shear resistance, with $R^2$, *MAE*, and *RMSE* values of 0.9642, 0.087 MN, and 0.126 MN, respectively. However, a comparison between experimental values and calculated values derived from classical analytical methods clearly demonstrates that existing design codes need to be improved. Additionally, Shapley additive explanations (SHAP) were applied to explain the model's predictions, with factors categorized according to their impact on failure modes and punching shear resistance. By modifying these parameters, punching resistance can be improved while reducing unpredictable failure. With the proposed hybrid algorithms, it is possible to determine the failure modes and the punching shear resistance of slabs during the preliminary stages of the construction.

**Keywords:** failure mode; punching shear resistance; machine learning; slab-column connection; hybrid algorithms



**Citation:** Yan, H.; Xie, N.; Shen, D. Hybrid Machine Learning Algorithms for Prediction of Failure Modes and Punching Resistance in Slab-Column Connections with Shear Reinforcement. *Buildings* **2024**, *14*, 1247. https://doi.org/10.3390/buildings14051247

Academic Editor: Francisco López-Almansa

Received: 3 April 2024
Revised: 22 April 2024
Accepted: 25 April 2024
Published: 28 April 2024



## 1. Introduction

Reinforced concrete (RC) slab-column connections are slabs supported directly on columns without beams, presenting a very simple construction method. As opposed to frame structures, flat slabs are prone to brittle punching failure, resulting in a limited capacity for deformation [1,2]. Since this type of failure occurs without any warning, alternative load paths cannot be guaranteed, resulting in progressive collapse [3]. The above-mentioned problems of the brittle failure mode can be mitigated by applying shear reinforcement, which must be capable of absorbing shear forces. Punching shear reinforcement is an effective method for enhancing ultimate strength and deformation capacity. Consequently, its use is encouraged in design codes, including the fib Model Code 2010 [4,5]. With its complex shear transfer mechanism, the main challenge is to accurately predict the failure modes and its corresponding punching shear resistance of RC slab-column connections [6].

The equations for shear design codes are derived from empirical expressions, such as ACI318-19 [7] and Eurocode 2 [8]. A formula that is not calibrated within the range may yield unsafe results, and engineers are still unfamiliar with the mechanics of punching shears. For estimating the shear capacity of slab-column connections, several theoretical

models have been developed, including the strut-and-tie model, the modified compression field theory, and the critical shear crack theory [9–14]. Due to their limited database and high influence of assumptions made during the derivative process, these models cannot be applied to a wide range of tests [15,16]. Considering the complexity involved in the shear transfer mechanism, the derivation and numerical implementation of the above models will be extremely challenging [17]. Also, it is not possible to conduct a systematic evaluation of concrete and shear reinforcements based on the additive approach used in most punching shear models [18,19].

According to Ashour et al. [20] and Bradford et al. [21], the ultimate strength and deformation capacity of slabs are influenced by the strength of the shear reinforcement and concrete. The tension reinforcement ratio, the slab depth, and the arrangement and amount of shear bars are also critical factors [22–25]. Even though slab's failure mode cannot be ignored, research on it has been limited [26,27]. When shear reinforcement is present, the critical crack might intersect the shear-bars and result in punching within shear reinforcement zone (Figure 1c). Critical cracks may occur be-neath the shear reinforcement and extend toward the tension face, away from the zone of the shear-bars and result in punching within the shear reinforcement zone (Figure 1d). The crushing of the compression strut may also result in punching shear failure between the column periphery and the first perimeter of the shear-bars (Figure 1b) [28,29]. Prior to punching shear resistance, it is essential to determine the failure modes of slabs, due to the fact that the types of failures are the result of different resistance mechanisms.

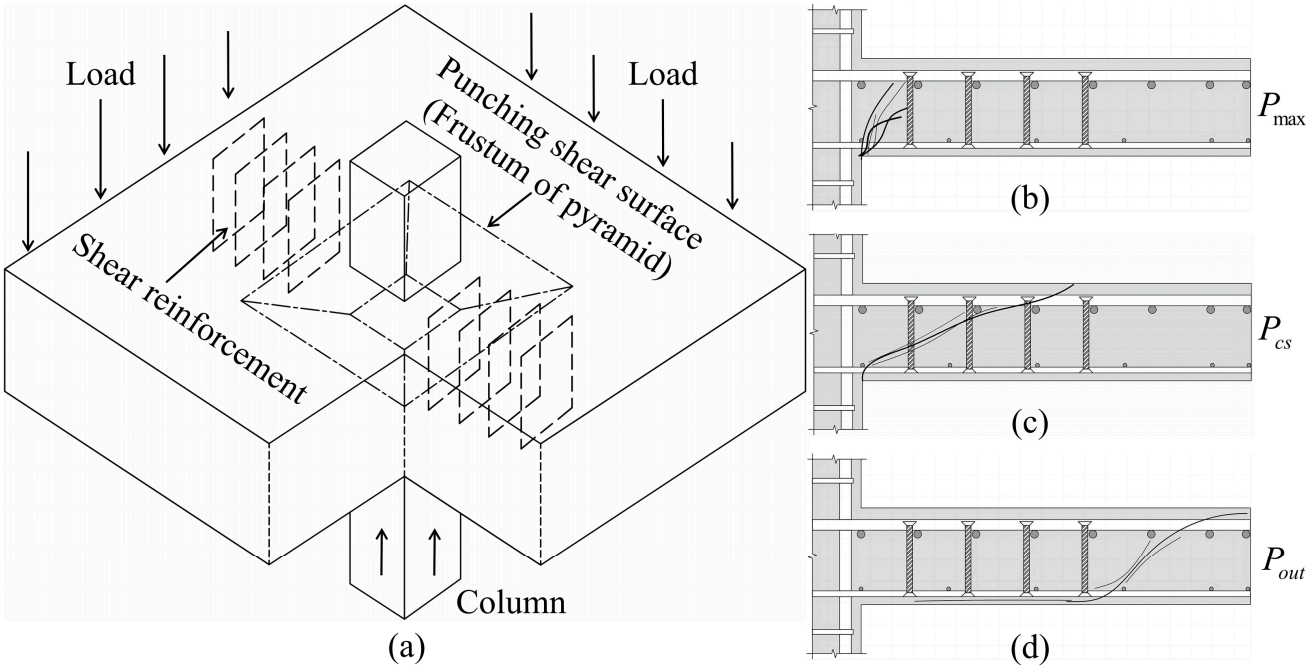


**Figure 1.** Types of failure: (**a**) slab-column connections with shear reinforcement; (**b**) crushing of compression strut; (**c**) failure within shear-reinforced zone; (**d**) failure outside shear-reinforced zone.

A variety of experimental studies have been conducted on the punching shear resistance of slab-column connections [30–35]; however, there are few studies that have focused on identifying failure modes. The influences that contribute to failure and the relationship between strain and stress prior to collapse are not fully understood. As mentioned above, due to some constraints, such as a lack of consideration of critical factors and simplifications of the equation-building process, the existing models are not capable of providing accurate predictions [36].

Machine learning (ML) approaches have recently become increasingly prevalent in structural engineering, ranging from fundamental mechanics-based models to purely

data-driven models [37]. Despite their differences in focus, some studies have demonstrated that both approaches are effective in resolving structural problems [38,39]. These studies can be categorized into two types: regression-based models (e.g., resistance) and classification-based models (e.g., failure modes). In light of this, Nguyen et al. [40] and Asgarkhani et al. [41] applied ML methods successfully to estimate the damaged state of the structures corresponding to residual limit states. The punching strength of slabs without shear reinforcement has recently been estimated using several ML algorithms. Akbarpour et al. [42] concluded that both artificial neural networks (ANN) and neuro-fuzzy inference models were capable of accurately predicting punching shear strength. Multiple linear regression (MLR) and artificial neural networks (ANN) were employed by Tran et al. for the analysis of two-way flat slabs [43]. Further studies were conducted using deep learning (DL), Gaussian Process Regression (GPR), bat-ANN algorithms, and support vector regression (SVR) [44–46]. It has been demonstrated that ML approaches are versatile and reliable; however, it is undeniable that the original model without parameter tuning has limitations [47].

Until recently, no studies have been conducted using ML approaches to determine the failure modes for shear-reinforced slabs. Even though ML-based models may produce more accurate results, only two studies have been conducted for slabs without shear reinforcement and have been limited to identifying the flexural failure and punching failure [11,48]. In this sense, the proposed methods may not be applicable to actual slab-column systems due to the lack of clarity on the failure mechanism of slabs with shear reinforcement. As long as the failure mode is accurately identified at the design stage, the brittle collapse of slab-column connections can be avoided. The use of ML models in engineering applications may be limited by the fact that although they are capable of learning from collected data, the actual modeling process may not always be obvious. This problem was solved by Mangalathu et al. [49] by using the SHAP method to explain the modeling process. It was then applied to various aspects of structural engineering, thereby encouraging the application of ML techniques [50–52]. Analyzing the importance of features can be used to determine the impact of input variables on prediction using machine learning techniques [53].

Based on the literature review above, this study presented a hybrid optimized model for identifying failure modes and predicting punching shear resistance of slab-column connections with shear reinforcement. As a first step, 328 sets of punching shear tests on slab-column connections are compiled from the literature. Following the development of three standard classifier algorithms (RF, LightGBM, XGBoost), the actual FM is used to develop regression models for the prediction of punching shear resistance using two hybrid optimized algorithms (WOA-XGBoost and GWO-XGBoost). In order to determine the predictive accuracy of the best-performing ML algorithm, it is compared to design provisions and actual values. It is possible to optimize the design of slabs by interpreting the results of the ML model using the SHAP.

This paper is organized as follows: A brief summary of the methodology used in this study is presented in Section 2. For slab-column connections with shear reinforcement, Section 3 presents a prediction of failure mode and punching shear resistance through hybrid optimized algorithms. Section 4 compares the ML-based predictions with existing methods, and SHAP is applied to determine a model explanation. There is a conclusion in Section 5 of this paper.

## 2. Methodology

### *2.1. Design Codes for Punching Resistance*

The punching shear resistance of slab-column connections with shear reinforcement are equal to the lowest values lowest figures of $V_{R,cs}$, $V_{R,out}$, and $V_{R,max}$, but cannot be less than that of similar slabs without shear reinforcement.

2.1.1. ACI 318 (2019)

Punching resistance is measured at a perimeter ($u_1$) $0.5d$ from the face of the column, in accordance with ACI 318-19 [7]. A formula for calculating the resistance in the failure mode of $P_{max}$ is provided in Equation (1).

$$V_{R,max} = 0.5\sqrt{f_c}u_1 d \tag{1}$$

The punching resistance in the failure mode of $P_{cs}$ and $P_{out}$ is calculated by applying the following equations to the control perimeters $u_1$ and $u_{out}$.

$$V_{R,cs} = 0.17\sqrt{f_c}u_1 d + \frac{A_{sw} f_{ywt} d}{S_r} \tag{2}$$

$$V_{R,out} = 0.17\sqrt{f_c}u_{out} d \tag{3}$$

where $f_c$ is the compressive strength of concrete cylinders, $d$ represents the effective depth of longitudinal reinforcement in the slab, $u_{out}$ is the critical perimeter measured from the last shear reinforcement perimeter by $0.5d$, $f_{ywt}$ represents the yield strength of shear reinforcement, and $S_r$ refers to the spacing between shear reinforcements.

2.1.2. Eurocode 2 (2004)

Punching resistance is measured at a perimeter ($u_0$) $2d$ from the face of the column, in accordance with Eurocode 2 [8]. A formula for calculating the resistance in the failure mode of $P_{max}$ is provided in Equation (4).

$$V_{R,max} = 0.24\left(1 - \frac{f_c}{250}\right) f_c u_0 d \tag{4}$$

The punching resistance in the failure mode of $P_{cs}$ and $P_{out}$ is calculated by applying the following equations to the control perimeters $u_0$ and $u_{out}$.

$$V_{R,cs} = 0.135k(100\rho f_c)^{\frac{1}{3}} u_0 d + 1.5\frac{A_{sw} f_{yw,ef} d}{S_r} \tag{5}$$

$$V_{R,out} = 0.18(100\rho f_c)^{\frac{1}{3}} u_{out} d \tag{6}$$

$$k = \left(1 + \sqrt{\frac{200}{d}}\right) \leq 2.0 \tag{7}$$

where $\rho$ represents the flexural reinforcement ratio, $k$ represents the size effect, and $f_{yw,ef}$ is the effective strength of the shear reinforcement. $u_{out}$ is the critical perimeter measured from the last shear reinforcement perimeter by $1.5d$.

*2.2. Overview of Standard Algorithms*

2.2.1. Random Forest (RF)

Random forest (RF) is a classifier composed of multiple decision trees; the output category is determined by each decision tree's mode [54]. It is possible to calculate the mean error between the test value and the mean predicted value under all sub-nodes by using the following equation.

$$F(x_n) = \frac{1}{k}\sum_{i=1}^{k}\left(y_{i,exp} - \frac{1}{k}\sum_{i=1}^{k} y_{i,pred}\right) \tag{8}$$

2.2.2. Light Gradient Boosting Machine (LightGBM)

LightGBM is a form of gradient boosting that relies on the decision tree, a highly effective approach for addressing regression and classification problems [55]. The subsequent

weak estimator can be trained by fitting the gradients of the previous weak estimator as the result of the LightGBM (Figure 2b). Leaf-wise algorithms select the leaf with maximum loss difference to grow, as demonstrated:

$$(p_k,\ f_k, v_k) = \text{argmin}_{(p,f,v)} L(T_{k-1}(X) split(p, f, v),\ Y) \tag{9}$$

$$T_k(X) = T_{k-1}(X)\ split(p_k,\ f_k, v_k) \tag{10}$$

where $k$ indicates the optimal solution, $p$ represents the current leaf node, $f$ stands for the division feature, and $v$ represents the segmentation value.

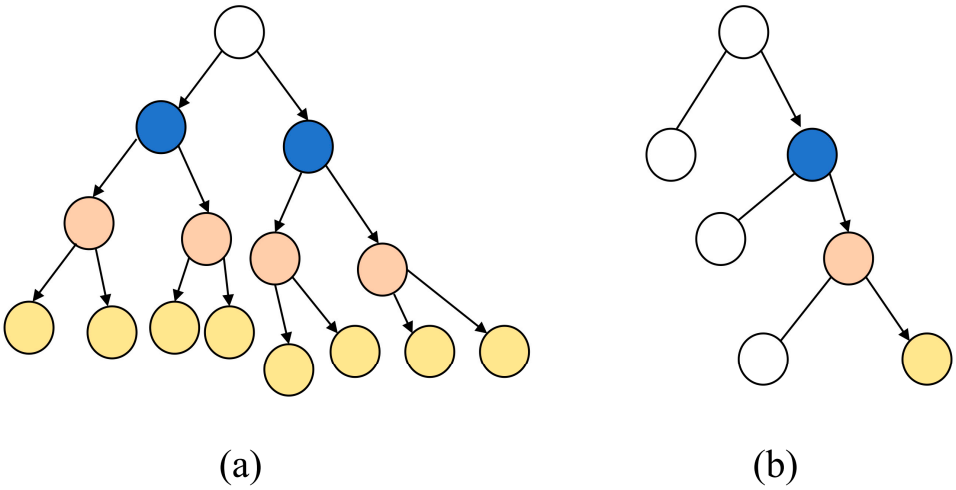


**Figure 2.** Algorithm visualizations for XGBoost and LightGBM: (**a**) level-wise tree growth in XGBoost; (**b**) leaf-wise tree growth.

#### 2.2.3. Extreme Gradient Boosting (XGBoost)

The extreme gradient boosting (XGBoost) model was proposed as part of the boosting ensemble ML approach in 2016 [56] which allows the model parameters to be continuously optimized via an objective function, thereby improving prediction accuracy. Figure 2a illustrates the algorithm visualization for XGBoost.

$$F_O(X_i,\ \hat{X}_i) = F_L(X_i,\ \hat{X}_i) + F_\Omega(X_i,\ \hat{X}_i) \tag{11}$$

$$\hat{X}_i = \sum_{i=1}^{M} \phi_m(x_i),\ \ \phi_m \in \Theta \tag{12}$$

where $F_O$, $F_L$, $F_\Omega$ represent the objective function, loss function and risk function, respectively. $M$ indicates the number of trees, and the $\phi_m$ represents the prediction score associated with the tree $m$; $\Theta$ refers to the boosting tree space.

### *2.3. Hybrid Optimized Algorithms*

#### 2.3.1. Grey Wolf Optimization (GWO)

Grey wolf optimization (GWO) [57,58] simulates grey wolves' social behavior by mimicking their hunting and leadership patterns. Grey wolves can be divided into four species, with the Alpha ($\alpha$) wolf serving as the pack leader, followed by Beta ($\beta$) and Delta ($\delta$) wolves, while Omega ($\omega$) wolves are at the bottom of the food chain (Figure 3a).

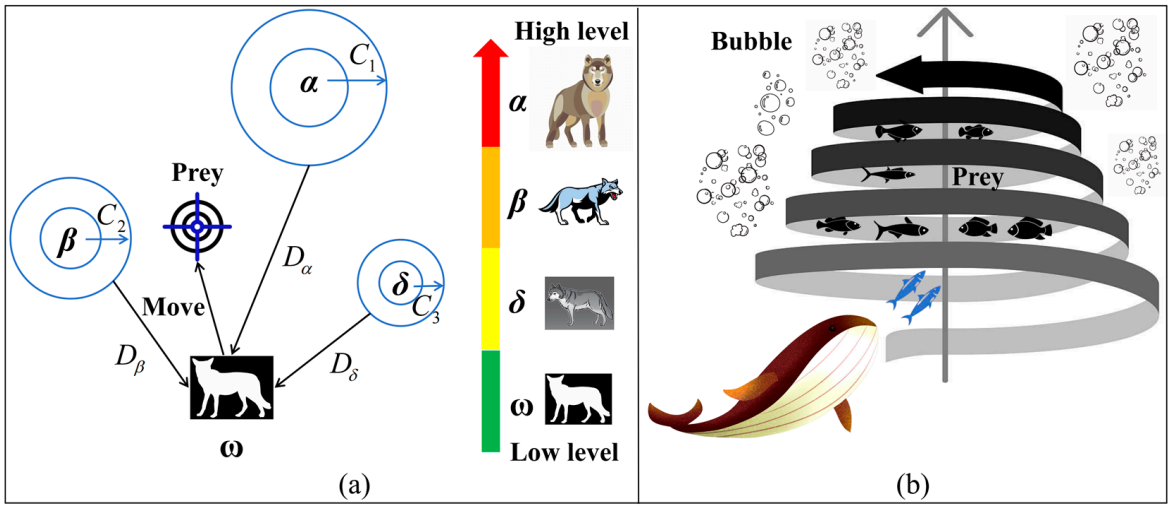


**Figure 3.** Hybrid optimized algorithms: (**a**) GWO; (**b**) WOA.

The hunting behavior involves searching, encircling, hunting, and attacking the prey, whose encircling can be determined as follows:

$$\begin{cases} \vec{D} = \left| \vec{C}\ \vec{P}_{xi} - \vec{P}_n \right| \\ \vec{P}_{n+1} = \vec{P}_{xi} - \vec{A}\ \vec{D} \end{cases} \tag{13}$$

where $\vec{A} = 2\vec{a}\ \vec{q}_1 - \vec{a}$, $\vec{C} = 2\vec{q}_2$, $\vec{a} = 2 - 2(t/t_{\max})$, the two random vectors $\vec{q}_1$ and $\vec{q}_2$ are in the range [0, 1], and $\vec{a}$ is a parameter that decreases linearly from 2 to 0 until ($t_{\max}$) has been reached. As $\left|\vec{A}\right| > 1$, diverting search agents will be employed, while exploitation is accomplished through the convergence of search agents in the case of $\left|\vec{A}\right| < 1$; [57] provides more detailed information on GWO algorithm.

2.3.2. Whale Optimization Algorithm (WOA)

The whale optimization algorithm is a meta-heuristic optimization approach derived from humpback whales' bubble-net feeding strategy [59]. There are three common foraging patterns: encircling, attacking with bubble nets, and hunting. Humpback whales encircle potential prey after finding it and updating their position (refer to Figure 3b) by the following equations:

$$\begin{cases} \vec{D} = \left| \vec{C}\ \vec{X}_{Oj} - \vec{X}_j \right| \\ \vec{X}_{j+1} = \vec{X}_{Oj} - \vec{N}\ \vec{D} \end{cases} \tag{14}$$

where in the $j$-th iteration, $\vec{X}_j$ represents the current position, and $\vec{X}_{Oj}$ represents the optimal position. The $\vec{C}$ and $\vec{D}$ are as follows:

$$\vec{C} = \left| 2\vec{a}\ \vec{q} - \vec{a} \right|, \ \vec{N} = 2\vec{q} \tag{15}$$

where the coefficient factor $\vec{a}$ decreases from 2 to 0, while the $\vec{q}$ represents the random number distribution between 0 and 1.

## 3. Implementation Procedures for Prediction

### *3.1. Database for Slab-Column Connection with Shear Reinforcement*

Data-driven models must be based on high-fidelity data, such as experimental data, in order to achieve high prediction accuracy. An in-depth literature review was conducted in order to investigate punching resistance and failure modes in slab-column connections with shear reinforcement configurations. Based on 328 experimental data points collected from publications [19,25,31,33,60–73], comparative models were created. The results of some studies [37,43,45–48] indicate that similar sized data sets may also be feasible, and they may produce accurate predictions. In this study, independent samples were collected from laboratory experiments performed on a two-way reinforced concrete slab with shear reinforcement. Data information is summarized in the Supplementary Materials, in which $d$ is the slab's effective depth; $a$ represents the radial distance from column face to the bearing point; as determined via ACI318-19, $c$ is the equivalent width of a column; $\rho_t$ stands for the ratio of flexural reinforcements; $b_0$ denotes the slab's critical perimeter located 0.5 $d$ from the column face; $A_{sw,d}$ is the cross sectional area of the shear reinforcement within the column face $d$, $f_{lc}$ is the concrete compression strength; $f_y$ refers the yield strength of the flexural reinforcement, $f_{y,sw}$ refers the yield strength of the shear bar; $V_{n,exp}$ is the punching resistance; and FM is the failure mode of the slabs ($P_{max}$ = 0, $P_{cs}$ = 1, and $P_{out}$ = 2). Shear reinforcement is typically composed of stirrups (Sti), bent up bars (BuB), stud rails (StR), hooks (Ho), shear bonds (SB), shear ladders (ShA), and double headed studs (DHS). An extensive selection of parameters is available in this database, with a high degree of dispersion. The most dangerous failure mode should be investigated when two failure modes occur at the same time.

### *3.2. Definitions for Input and Output Variables*

To conduct further analysis, input and output variables must be determined. In terms of classification and regression, these are two distinct problems. In the FM classification, there are nine input variables, and the output variable is the mode of failure of slabs (Table 1). Additionally, according to references [60–72], these input variables have a significant influence on failure modes and the punching resistance of slabs. The actual FM is considered as an input variable in the resistance regression, resulting in ten input variables and one output variable.

**Table 1.** Summary information of the variables.

| Notation | Unit | Parameters | Type | |
|---|---|---|---|---|
| | | | FM | Resistance |
| $d$ | m | $x_1$: Effective depth of the slab | Input | Input |
| $a/d$ | - | $x_2$: Span to effective depth ratio | Input | Input |
| $c/b_0$ | - | $x_3$: Column width to critical perimeter ratio | Input | Input |
| $b_0/d$ | - | $x_4$: Critical perimeter to effective depth ratio | Input | Input |
| $\rho_t$ | % | $x_5$: Flexural reinforcement ratio | Input | Input |
| $A_{sw,d}$ | $cm^2$ | $x_6$: Cross-section area of the shear reinforcement | Input | Input |
| $f_{lc}$ | MPa | $x_7$: Concrete compression strength | Input | Input |
| $f_y$ | MPa | $x_8$: The yield strength of the flexural reinforcement | Input | Input |
| $f_{y,sw}$ | MPa | $x_9$: The yield strength of the shear reinforcement | Input | Input |
| FM | - | $y_1$: Failure mode | Output | Input |
| $V_{n,exp}$ | MN | $y_2$: Punching shear resistance | | Output |

### 3.3. Data Normalization

Prior to training, the input variables should be normalized since the extracted data have different units and ranges. As part of the normalization process, features are scaled on a similar basis [74]. By using the following normalization procedure, statistical bias can be reduced and machine learning models can be made more reliable:

$$X_{i,normal} = \frac{X_i - X_{min}}{X_{max} - X_{min}} \quad (16)$$

where the values of $X_{min}$ and $X_{max}$ represent the minimum and maximum values of respective input values.

### 3.4. Development of ML Models

As part of the process of developing a ML-based model for classification, the following steps should be followed: (1) preparation of data with input variables; (2) normalization of data; (3) in this study, the data set has been divided into two types: a training set (80%) and a testing set (20%); (4) training has been conducted using three standard machine learning models (RF, LightGBM, and XGBoost); (5) selecting the most accurate classification model; (6) obtaining the results of the prediction for the testing set. The actual FM is used as an input variable in the development of hybrid optimized ML algorithms (GWO-XGBoost, WOA-XGBoost) that can be used to assess the impact of different failure modes on punching resistance capacity (Figure 4). Following Figure 4, the best regression models to punching shear resistance have been developed for slab-column connections with shear reinforcement. The optimized parameters for regression models are also shown.

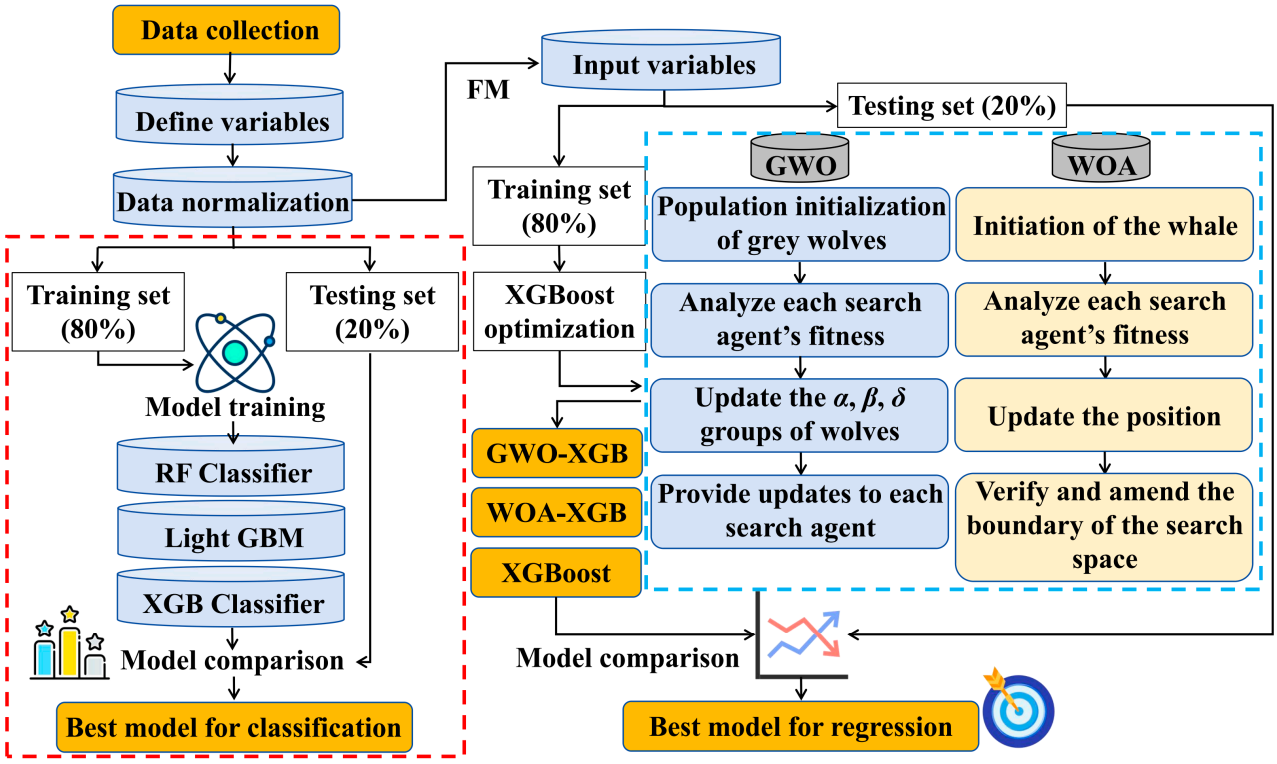


**Figure 4.** Flowchart for ML algorithm implementation.

There are three different failure modes, with $P_{max}$ = 69, $P_{cs}$ = 200, and $P_{out}$ = 59, respectively. Due to this unequal distribution of the database, there is the possibility of skew problems, which may also affect the calculation results. In this paper, the (scale_pos_weights) value of ML algorithms are adjusted to avoid bias in the experimental dataset. As a result

of this design, the ratio of different failure modes will remain the same during the training of each model. Some research studies have adopted the same approach as well [11,48].

### *3.5. Grid Search for Classifiers*

As shown in Figure 5, a grid search with 5-fold cross validation is used in this study. Once the appropriate parameters have been selected for each ML model, they are used to train the data and construct models for identifying failure modes. The predictive performance is evaluated using a test dataset following 5-fold cross-validation training. By further validating each iteration with an independent dataset, overfitting concerns could be mitigated. Model performance is evaluated using several metrics, which are presented in the following sections, including the classification confusion matrix, accuracy precision, and recall. Table 2 shows the main parameters for classifiers.

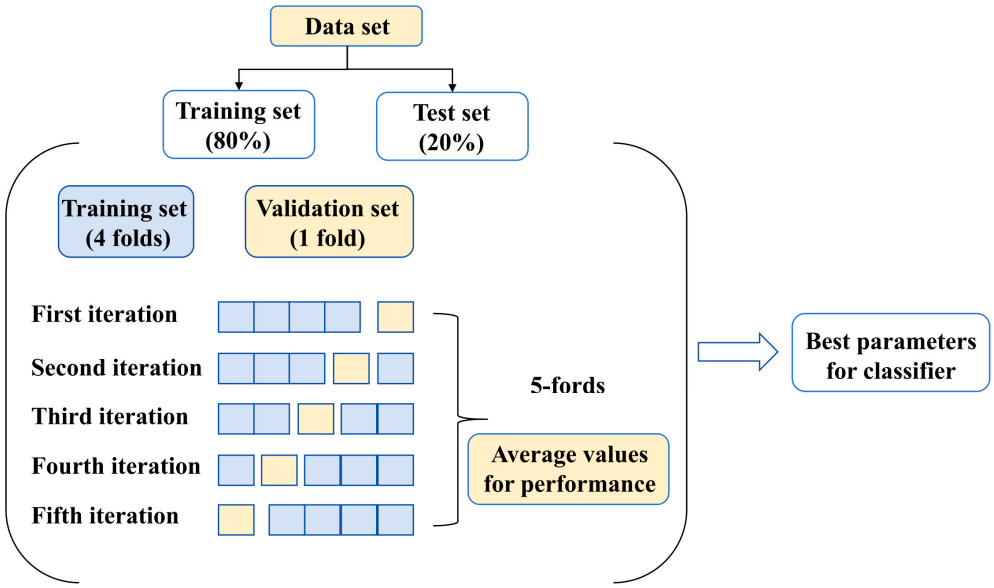


**Figure 5.** Grid search with 5-fold cross-validation.

**Table 2.** Main parameters for classification model.

| ML Algorithms | Main Parameters |
|---|---|
| RF classifier | Number of estimators = '103'; Maximum depth = '10'. |
| LightGBM | Number of estimators = '247'; Maximum depth = '7'; Learning rate = '0.6259' |
| XGBoost classifier | Number of estimators = '38'; Maximum depth = '4'; Learning rate = '0.6022'. |

### *3.6. Hybrid Optimization Process for Regression Analysis*

A comparison of the convergence curves of the hybrid algorithms (GWO-XGBoost and WOA-XGBoost) is shown in Figure 6. According to the results, the WOA-XGBoost model performed better during training (Swarm = 75, $R^2$ = 0.9645 in Figure 6a). Despite similar shapes, convergence curves for the WOA present a faster rate of convergence. The WOA achieves the best comprehensive performance not only during training, but also during the testing of *MAE*, *RMSE*, and $R^2$. Table 3 lists the main parameters of regression models.

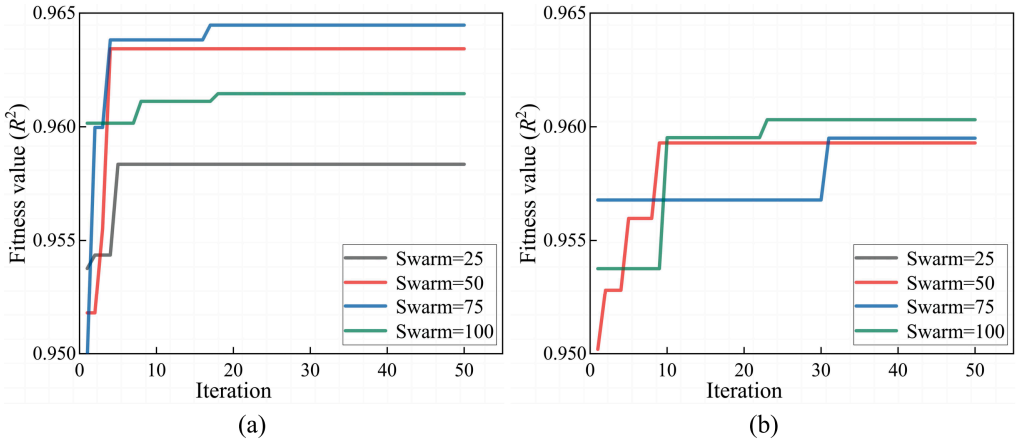


**Figure 6.** Convergence curves of the hybrid algorithms: (**a**) WOA; (**b**) GWO.

**Table 3.** Main parameters for regression models.

| ML Algorithms | Main Parameters |
|---|---|
| XGBoost | Number of estimators = '20'; Maximum depth = '3'; Learning rate = '0.1'; Objective = 'linear'; Booster = 'gbtree'. |
| GWO-XGBoost | Number of estimators = '183'; Maximum depth = '10'; Learning rate = '1.3205'; Objective = 'linear'; Booster = 'gbtree'. |
| WOA-XGBoost | Number of estimators = '85'; Maximum depth = '3'; Learning rate = '0.2008'; Objective = 'linear'; Booster = 'gbtree'. |

### *3.7. Measurement of Performance*

Three performance metrics are used in classification to evaluate the effectiveness of predictive models, including precision (*P*), recall (*R*), and accuracy (*Acc*). As part of regression, three performance measures are considered: the mean absolute error (*MAE*), the root mean square error (*RMSE*), and the coefficient of determination ($R^2$).

$$P = \frac{TP}{TP + FP} \tag{17}$$

$$R = \frac{TP}{TP + FN} \tag{18}$$

$$Acc = \frac{TP + TN}{TP + FP + TN + FN} \tag{19}$$

$$MAE = \frac{1}{n}\sum_{i=1}^{n}\left|y_{pre,i} - y_{exp,i}\right| \tag{20}$$

$$RMSE = \sqrt{\frac{1}{n}\sum_{i=1}^{n}\left(y_{pre,i} - y_{exp,i}\right)^2} \tag{21}$$

$$R^2 = 1 - \frac{\sum_{i=1}^{n}\left(y_{pre,i} - y_{exp,i}\right)^2}{\sum_{i=1}^{n}\left(y_{exp,i} - \frac{1}{n}\sum_{i=1}^{n} y_{exp,i}\right)^2} \tag{22}$$

where true positive (*TP*) is the number of accurately predicted failures for a given label, based on three types of failure modes: the crushing of the compression strut ($P_{max}$), failure within the shear reinforced zone ($P_{cs}$), and failure outside the shear-reinforced zone ($P_{out}$). False positive (*FP*) refers to the number of incorrect predictions associated with the same label. As opposed to *TN*, which represents true negative, *FN* represents false negative, which represents the number of incorrect predictions made by the other labels. $y_{exp,i}$ and

$y_{exp,i}$ are the predicted and actual values, respectively. Originally, the above expressions were proposed for two-class classification problems. The macro-average should be used when dealing with multiclass classification problems.

## 4. Results and Discussion

### *4.1. Prediction Results for Failure Modes*

Figure 7 illustrates the prediction results using a confusion matrix. In general, diagonal elements indicate failure modes that have been correctly classified using machine learning approaches, while other elements indicate failed predictions [75]. Accuracy (*Acc*) refers to the degree of accuracy with which each of the three possible failure modes can be predicted. The precision (*P*) is defined as the percentage of correct predictions for each predicted failure mode, while the recall (*R*) is defined as the percentage of correct predictions for each real failure mode.

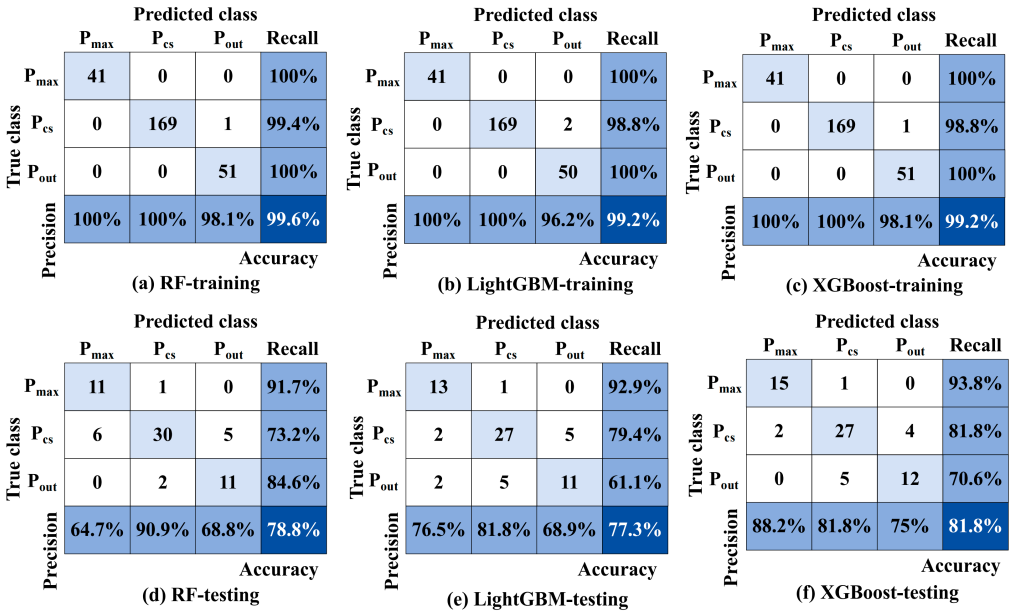


**Figure 7.** Failure mode classification based on ML approaches: (**a**) RF-training; (**b**) LightGBM-training; (**c**) XGBoost-training; (**d**) RF-testing; (**e**) LightGBM-testing; (**f**) XGBoost-testing.

The results indicate that XGBoost classifier had the highest accuracy rate, and that its precision and recall were also the highest in the training and testing datasets. According to the test results, $P_{max}$, $P_{cs}$, and $P_{out}$ have precisions of 88.2%, 81.8%, and 75%, respectively, and recalls of 93.8%, 81.8%, and 70.6%, respectively. Almost all of the failure modes are correctly classified in the training process. According to the bottom right corner of the diagram, the XGBoost classifier achieves an accuracy of 81.8%, which is better than RF and LightGBM. This may be due to the fact that the objective function and row and column sampling technique in XGBoost are designed to prevent overfitting. The branching metric is reset to a gain in structure score when the growth direction is more straightforward. While LightGBM is intended for large datasets, it is extremely sensitive to overfitting in small datasets. Figure 7 indicates that the recall for predicting the failure modes of $P_{cs}$ and $P_{out}$ is lower than that for $P_{max}$, primarily due to the complex mechanism of the $P_{cs}$ and $P_{out}$ and the differences between them during the testing not being well defined, which requires additional investigation.

### *4.2. Prediction Results for Punching Shear Resistance*

#### 4.2.1. Hybrid Model Performance under Optimization

As shown in Table 4, the predicted results are compared to the actual results. With $R^2$, *MAE*, and *RMSE* values of 0.9642, 0.087 MN, and 0.126 MN in the testing process, the WOA-

XGBoost demonstrated the best performance in predicting the punching shear resistance. In comparison to the standalone XGBoost, the GWO-XGBoost and WOA-XGBoost models demonstrate better performance. Accordingly, using hybrid optimized algorithms (GWO and WOA) to optimize the initial weights and biases can improve the performance of the hyperparameter determination process. With this method, the hyperparameters of the XGBoost algorithm are found to be well converged and an appropriate solution is obtained.

**Table 4.** Performance comparison of regression models.

| ML Algorithms | Training | | | Testing | | |
|---|---|---|---|---|---|---|
| | *MAE* (MN) | *RMSE* (MN) | $R^2$ | *MAE* (MN) | *RMSE* (MN) | $R^2$ |
| XGBoost | 0.125 | 0.203 | 0.884 | 0.149 | 0.242 | 0.8682 |
| GWO-XGBoost | 0.001 | 0.002 | 0.999 | 0.094 | 0.133 | 0.9603 |
| WOA-XGBoost | 0.033 | 0.045 | 0.994 | 0.087 | 0.126 | 0.9642 |

#### 4.2.2. Comparison with Empirical Models for Resistance

On Figure 8, the current design codes are compared with ML-based models. In terms of prediction performance, ML-based models outperform empirical models significantly. As shown in Table 5, the proposed WOA-XGBoost produces the most effective results, with smaller error metrics *MAE* and *RMSE* as well as higher correlation coefficients $R^2$. A hybrid algorithm may be able to (1) capture complex nonlinear mapping relationships between input variables and punching shear resistance; (2) and use the failure mode as a variable to predict the punching shear resistance, which may improve the accuracy of prediction.

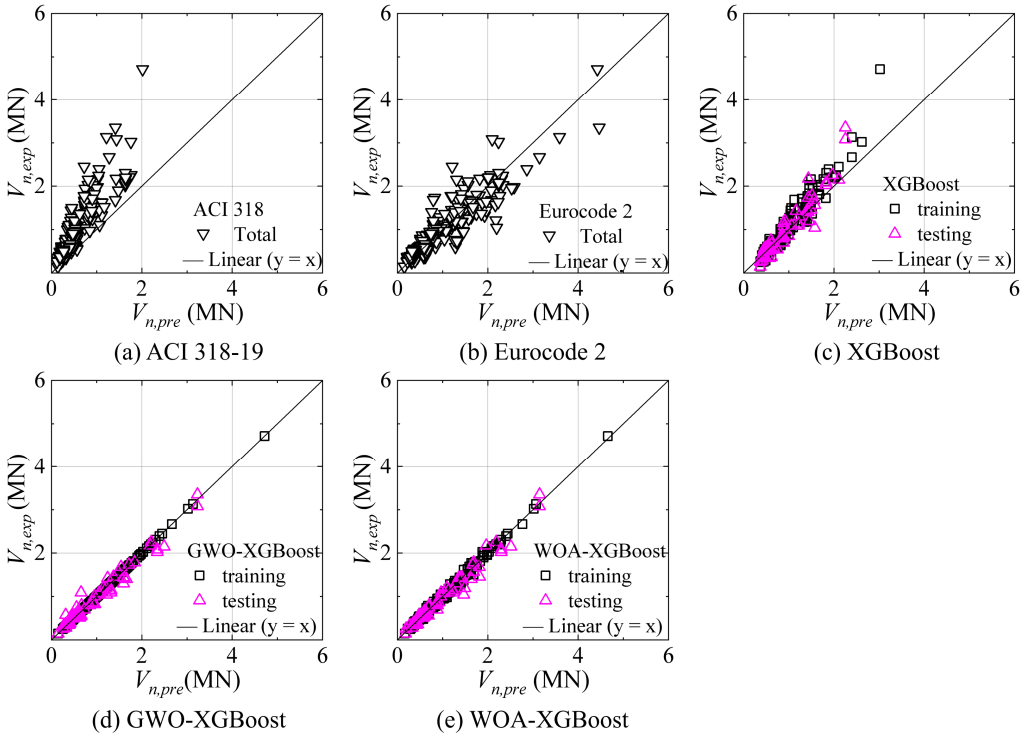


**Figure 8.** Comparison with existing methods: (**a**) ACI 318-19; (**b**) Eurocode 2-2004; (**c**) XGBoost; (**d**) GWO-XGBoost; (**e**) WOA-XGBoost.

**Table 5.** Summary of punching shear resistance.

| Model | AVG ($V_{n,exp}/V_{n,pre}$) | COV ($V_{n,exp}/V_{n,pre}$) | $R^2$ | *MAE* (MN) | *RMSE* (MN) |
|---|---|---|---|---|---|
| ACI 318-19 | 1.83 | 0.23 | 0.67 | 0.41 | 0.53 |
| Eurocode 2 | 1.09 | 0.22 | 0.81 | 0.17 | 0.26 |
| XGBoost (testing) | 1.02 | 0.18 | 0.8682 | 0.149 | 0.242 |
| GWO-XGBoost (testing) | 1.003 | 0.077 | 0.9603 | 0.094 | 0.133 |
| WOA-XGBoost (testing) | 0.995 | 0.071 | 0.964 | 0.087 | 0.126 |

Furthermore, the average value (AVG) and coefficient of variation (COV) of the ($V_{n,exp}/V_{n,pre}$) ratio are reported. ACI 318-19 [7] has been shown to be the most conservative in predicting punching shear resistance for slabs with shear reinforcement. It was found that the experimental results were more closely matched by the equations in Eurocode 2 since it calculates the punching shear capacity by taking into account both the shear and flexural reinforcements as well as the concrete [76]. In contrast to the assumption made in most design codes, concrete may not provide consistent resistance to slab-column connections. In the case of low amounts of shear reinforcement, most design codes underestimate this contribution whereas in the case of large amounts, they overestimate it [24]. It appears that the design equations may have been over simplified, and that some influential factors should be taken into account.

### *4.3. Model Explanation*

#### 4.3.1. SHAP Theory

The SHAP theory is a widely used interpretation model based on game theory [77]. Using the SHAP value, each feature contributes to the prediction result, and the output model is formed by adding the input variables linearly.

$$F(x) = G(x') = \delta_0 + \sum_{i=1}^{n} \delta_i x_i\prime \tag{23}$$

$$\delta_i(f, x) = \sum_{z \in x\prime} \frac{|z|(M - |z| - 1)!}{M!}[f_x(z) - f_x(z \setminus i)] \tag{24}$$

where $n$ stands for the number of inputs, and $S$ is the constant value in the absence of all inputs. $|z|$ represents the number of non-zero entries in $z$ ($z \in x\prime$), $z$ and $z \in x\prime$, and $\delta_i$ is the SHAP value. Each SHAP value depicts the change in the anticipated model prediction when the feature is conditioned. SHAP can be further explained in previous studies [78,79].

#### 4.3.2. Sensitivity Analysis for Failure Modes

The SHAP theory was used to determine the sensitivity of the variables affecting types of failure. Figure 9 illustrates the importance of input variables through a visual representation, and each variable contributes to a varying degree to the prediction. It provides additional information regarding slab failure modes that has not previously been examined. Previously published studies [11,20,22,48] focused more on global failure mode than on individual classes ($P_{max}$, $P_{cs}$, or $P_{out}$). According to Figure 9, $A_{sw,d}$ and $(a/d)$ have been found to be the two variables that are of highest importance in all three types of failures. There is a significant impact of $f_y$ on the failure mode $P_{max}$, while its effect on the two other failure modes is relatively minimal. The failure mode $P_{out}$ is significantly influenced by $d$, whereas its impact on the other two failure modes is relatively limited. These two parameters can also be used to determine a simple indicator of different failure modes.

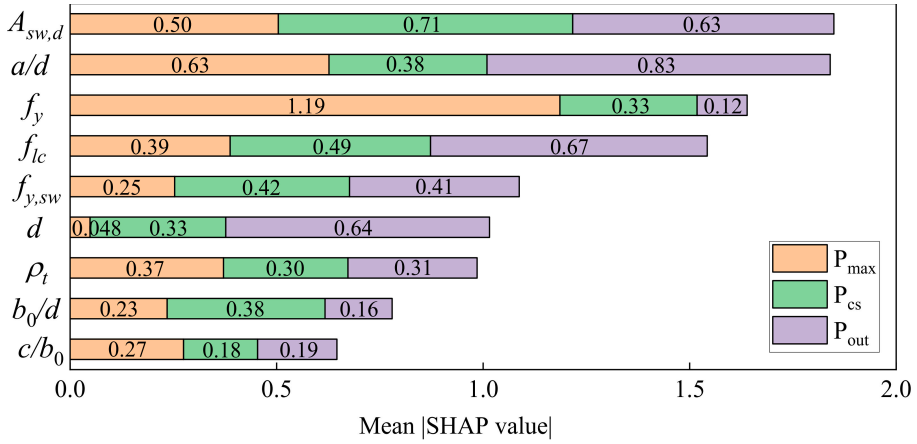


**Figure 9.** Feature importance for three failure modes using SHAP value.

#### 4.3.3. Summary Plots of the Failure Modes

The XGBoost classifier was selected as the model for interpretation using SHAP as it has the greatest ability in Section 4.1. Figure 10 shows the specific effect of each input variable on failure mode, where the colors from blue to red correspond to the size of the value from small to large. In order to assess the activation of the shear reinforcements and their contribution to punching shear resistance, the following analysis is conducted on $P_{cs}$. In Figure 10b, the four variables ($f_{lc}$, $\rho_t$, $d$, and $b_0/d$) have a positive effect on predictions, which means that slabs fail more frequently in $P_{cs}$ if those four variables are high. The four input variables ($A_{sw,d}$, $a/d$, $f_{y,sw}$, and $f_y$) have a negative effect, while there is no obvious influence on the $(c/b_0)$. Several studies [32,80] have demonstrated a positive effect of the $\rho_t$ of the slab on the formation of punching shear cones. This also explains why thick slabs with a high flexural reinforcement ratio fail in punching shear, even if they are shear-reinforced [28].

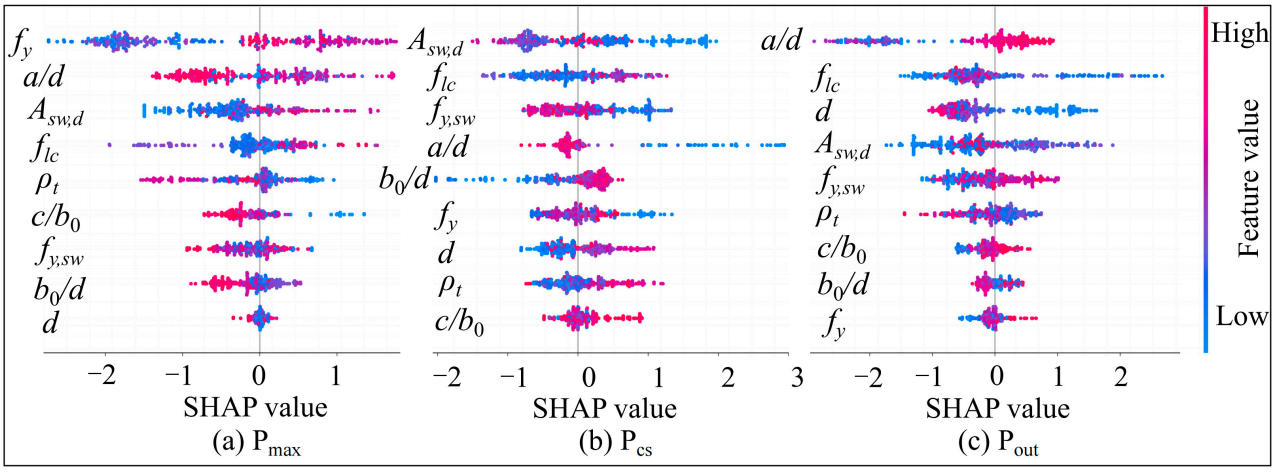


**Figure 10.** Summary plots of SHAP values for three types of failure.

#### 4.3.4. Sensitivity Analysis of the Punching Shear Resistance

WOA-XGBoost was selected as the most accurate model in this research, and SHAP was used to interpret the results. The feature importance for each of the ten input variables is presented in Figure 11a. The most sensitive variable is $d$, followed by $A_{sw,d}$, $\rho_t$, $(a/d)$, $f_{lc}$, $(c/b_0)$, $f_y$, $f_{y,sw}$, $(b_0/d)$, and FM. As a result, it is evident that improving $A_{sw,d}$ and $\rho_t$ is a more effective way of enhancing punching shear resistance than increasing $f_{y,sw}$ and $f_y$. Although FM contributes the least to punching resistance, it cannot be ignored due to its

close relationship to the other input variables in Figure 9. After incorporating FM into the data-driven model, the punching resistance can be predicted more accurately.

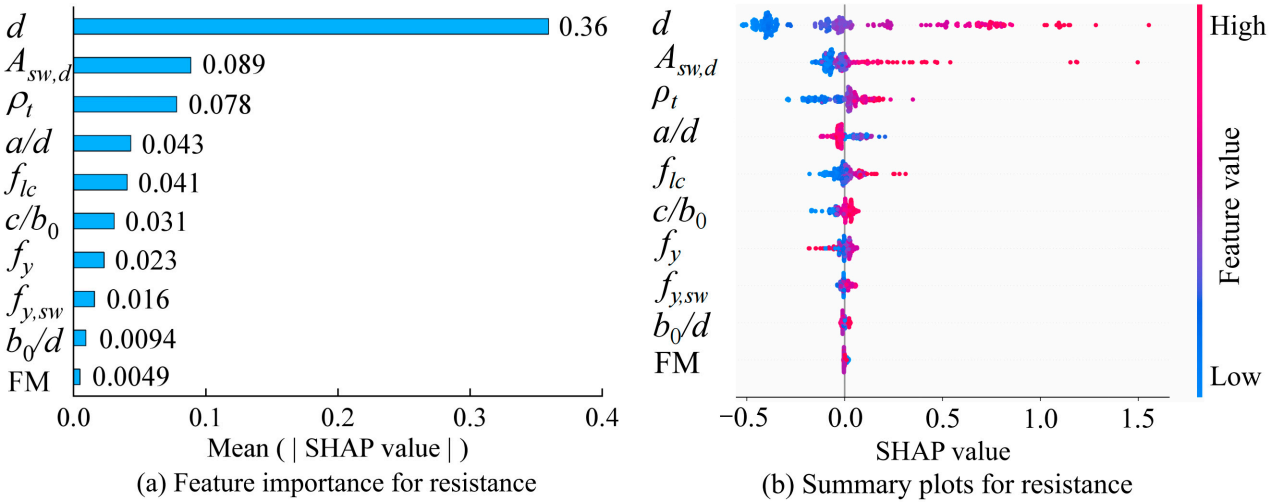


**Figure 11.** Global interpretations using SHAP: (**a**) feature importance for resistance; (**b**) summary plots for resistance.

As shown in Figure 11b, punching resistance increases as these seven variables ($d$, $A_{sw,d}$, $\rho_t$, $f_{lc}$, $c/b_0$, $f_{y,sw}$, $b_0/d$) are increased, while ($a/d$, $f_y$) are decreased. As can be seen, increasing $\rho_t$ and $f_{lc}$ not only improves punching resistance, but also reduces the risk of the failure mode in $P_{max}$ and $P_{out}$ (refer to Figure 10). Increasing $d$ reduces the risk of $P_{out}$ failure (Figure 10c), and because of the shear bars, the failure mode of those slabs is more likely to be $P_{cs}$. The use of $(c/b_0)$ to increase punching resistance could increase the risk of $P_{out}$ failure, so this consideration should be taken into account when designing this parameter. The increase in the $(a/d)$ not only reduces the resistance, but also increases the risk of failure of the $P_{out}$, which should be avoided. Furthermore, it has been shown that the punching shear resistance decreases as $f_y$ increases [43], which might be explained by widening shear cracks and, therefore, a reduced contribution of concrete to punching shear capacity.

#### 4.3.5. Feature Dependency of the Punching Shear Resistance

This section presents the six most sensitive factors (refer to Figure 11a) for resistance and demonstrates the validity of WOA-XGBoost's prediction based on SHAP. In Figure 12, feature dependency plots are shown for punching shear resistance. Increasing $d$, $A_{sw,d}$, $\rho_t$, $f_{lc}$, and $(c/b_0)$ values result in an increase in SHAP values, while decreasing the $(a/d)$ value results in an increase in SHAP values.

Increasing the effective depth of a slab improves the punching shear resistance, particularly if the $d$ exceeds 180 mm (Figure 12a). Experiments have also demonstrated the effect of $d$ on punching capacity [22,33]. Furthermore, ACI 318-19 and Eurocode 2-2004 provide unconservative predictions for slabs with $d$ wider than 200 mm, whereas they provide improved prediction for slabs with $d$ less than 200 mm, which should be improved [81]. A change in the SHAP value was observed from (−0.25) to (+1.50), as the $A_{sw,d}$ grew between 0 and 100 cm$^2$. $A_{sw,d}$ positively influences punching resistance if it is wider than 20 cm$^2$. According to a prior study [46], if $\rho_t$ is too small, the slab will fail when the shear bars are not fully worked, the slab will fail the shear bars that are being fully worked, which should be avoided. Based on Figure 12c, the SHAP value will be greater than zero if $\rho_t$ exceeds 1%, which results in an increase in the punching shear resistance. Nevertheless, the ACI 318 code often fails to take notice of this. EC2-2004 and ACI 318-19 do not take into consideration both $(a/d, c/b_0)$ when calculating punching resistance. As can be seen in Figure 12b, the SHAP value increased whereas $(a/d)$ decreased from 10 to 2. In particular,

an $(a/d)$ less than 5 has a positive impact on punching resistance. It may be explained by the development of arch mechanisms in slabs and the effects of friction at the support [82]. When $(c/b_0)$ increases on a slab, the SHAP value increases from $(-0.15)$ to $(+0.05)$ in Figure 12f as $(c/b_0)$ exceeds 0.15, having a positive effect on punching resistance. The $(c/b_0)$ value is critical in limiting the formation on the punching shear cone, however, current design methods tend to ignore this factor. A reduction in the SHAP value occurs when concrete compressive strength decreases (Figure 12e); it has a positive impact on punching shear resistance when the value of $f_{lc}$ exceeds 38 MPa. The size and width of concrete cracks may increase with decreasing concrete strength under punching loads, due to the reduced possibility of interlocking between aggregate gains on opposite sides of the crack.

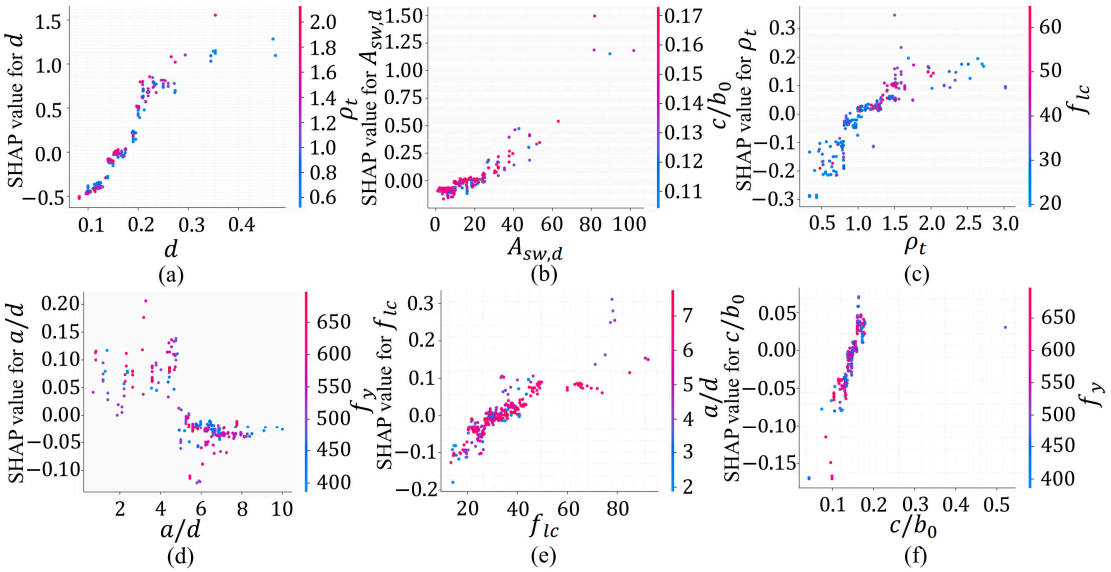


**Figure 12.** Feature dependency plots for punching resistance using SHAP values: (**a**) $d$; (**b**) $A_{sw,d}$; (**c**) $\rho_t$; (**d**) $a/d$; (**e**) $f_{lc}$; (**f**) $c/b_0$.

In conclusion, the feature importance analysis indicates that ($d > 180$ mm, $A_{sw,d} > 20$ cm$^2$, $\rho_t > 1\%$, $c/b_0 > 0.15$, $f_{lc} > 38$ MPa, $a/d < 5$), all of which are positively correlated with punching shear resistance in slab-column connections with shear reinforcement.

### *4.4. Limitations*

This study has improved the accuracy of predicting punching shear resistance and failure modes using ML models; however, there are some limitations that deserve further attention. Depending on the characteristics of the collected datasets, the classification and regression results of this study could be limited in their generalizability to broader scenarios. Including a larger range of databases that represent a variety of structural configurations, geometric characteristics, and material properties could provide a more comprehensive outcome. Despite the fact that the model performs well in terms of punching shear resistance, much work remains to be performed in order to better identify the failure modes of many slab-column connections, to lead to a decrease in the model's reliability. The authors expect to conduct future research in this area.

## 5. Conclusions

Since the force transmission mechanism of the slab-column connection with shear reinforcement is complex, it has always been challenging to predict the failure mode in advance. An interpretable data-driven model has been developed for analyzing the failure modes using three typical ML models, RF, LightGBM, XGBoost, and compared to develop a robust classification technique. Additionally, a prediction method for punching shear resistance that considers slab failure modes was proposed using two hybrid algo-

rithms (GWO-XGBoost and WOA-XGBoost). This study revealed a number of interesting findings, including:

1. In failure mode classification, the XGBoost classifier achieves the highest accuracy rate of almost 81.8%, thus filling the gap caused by the lack of empirical formulae.
2. There is a significant impact of $f_y$ the on the failure mode $P_{max}$, while the failure mode $P_{out}$ is significantly influenced by $d$. These two parameters can also be used to determine a simple indicator of different failure modes.
3. In the punching shear resistance prediction, the proposed WOA-XGBoost produced the most effective results in testing, due to the fact that the effect of the failure modes has been taken into consideration.
4. The performance of hyperparameter determination can be improved by using hybrid algorithms (GWO and WOA).
5. The feature importance analysis indicates that ($d > 180$ mm, $A_{sw,d} > 20$ cm$^2$, $\rho_t > 1\%$, $c/b_0 > 0.15$, $f_{lc} > 38$ MPa, $a/d < 5$) are positively correlated with punching shear resistance.
6. As a result of SHAP explanations, a number of parameters that influence failure modes and punching resistance have been identified, and by altering these parameters punching resistance can be improved while brittle collapse is reduced.

**Supplementary Materials:** The following supporting information can be downloaded at: https://www.mdpi.com/article/10.3390/buildings14051247/s1, Excel S1. References [19,25,31,33,60–73] are cited in the supplementary materials.

**Author Contributions:** H.Y.: Investigation, methodology, writing—original draft and project administration. N.X.: Supervision. D.S.: Software. All authors have read and agreed to the published version of the manuscript.

**Funding:** This research received no external funding.

**Data Availability Statement:** All data that support the findings of this study are available from the corresponding author upon reasonable request.

**Conflicts of Interest:** Author Dandan Shen was employed by the company SANY Heavy Industry Co., Ltd. The remaining authors declare that the research was conducted in the absence of any commercial or financial relationships that could be construed as a potential conflict of interest.

## References

1. Jiao, Z.Y.; Li, Y.; Guan, H.; Diao, M.Z.; Wang, J.K.; Li, Y.C. Pre-and post-punching failure performances of flat slab-column joints with drop panels and shear studs. *Eng. Fail. Anal.* **2022**, *104*, 106604. [CrossRef]
2. Diao, M.Z.; Li, Y.; Guan, H.; Lu, X.Z.; Gilbert, B.P. Influence of horizontal restraints on the behavior of vertical disproportionate collapse of RC moment frames. *Eng. Fail. Anal.* **2019**, *109*, 104324. [CrossRef]
3. Najmi, A.Q.; Al-Ateyat, A.; Allouzi, R. Analysis of reinforced concrete plates with swimmer bars as punching shear reinforcement. *Proc. Inst. Civ. Eng. Struct. Build.* **2021**, *174*, 920–933. [CrossRef]
4. Hegger, J.; Sherif, A.G.; Kueres, D.; Siburg, C. Efficiency of Various Punching Shear Reinforcement Systems for Flat Slabs. *ACI Struct. J.* **2017**, *114*, 631–642. [CrossRef]
5. FIB (Fédération Internationale du Béton Lausanne, Switzerland). *FIB Model Code for Concrete Structures*; Wiley-Blackwell: Berlin, Germany, 2010.
6. Ju, M.; Ju, J.W.W.; Sim, J. A new formula of punching shear strength for fiber reinforced polymer (FRP) or steel reinforced two-way concrete slabs. *Compos. Struct.* **2021**, *259*, 11347. [CrossRef]
7. *ACI 318*; Building Code Requirements for Structural Concrete and Commentary. ACI: Farmington Hills, MI, USA, 2019.
8. *EN 1992*; Eurocode 2: Design of Concrete Structures-Part 1-1: General Rules and Rules for Buildings. European Committee for Standardization: Brussels, Belgium, 2004.
9. Sahoo, S.; Singh, B. Punching shear capacity of recycled-aggregate concrete slab-column connections. *J. Build. Eng.* **2021**, *41*, 102430. [CrossRef]
10. Sahoo, S.; Singh, B. Punching shear capacity of steel-fibre recycled aggregate concrete slab. *Mag. Concr. Res.* **2022**, *72*, 865–878. [CrossRef]
11. Liang, S.X.; Shen, Y.X.; Gao, X.L.; Cai, Y.Q.; Fei, Z.Y. Symbolic machine learning improved MCFT model for punching shear resistance of FRP-reinforced concrete slabs. *J. Build. Eng.* **2023**, *69*, 106257. [CrossRef]

12. Nana, W.S.A.; Bui, T.T.; Bost, M.; Limam, A. Shear Bearing Capacity of RC Slabs without Shear Reinforcement: Design Codes Comparison. *KSCE J. Civ. Eng.* **2019**, *23*, 321–334. [CrossRef]
13. dos Santos, J.B.; Muttoni, A.; de Melo, G.S. Enhancement of the punching shear verification of slabs with opening. *Struct. Concr.* **2023**, *24*, 3021–3038. [CrossRef]
14. Deifalla, A. Punching shear strength and deformation for FRP-reinforced concrete slabs without shear reinforcements. *Case Stud. Const. Mat.* **2022**, *16*, e00925. [CrossRef]
15. Salehi, H.; Burgueno, R. Emerging artificial intelligence methods in structural engineering. *Eng. Struct.* **2018**, *171*, 170–189. [CrossRef]
16. Luo, H.; Paal, S.G. Machine Learning-Based Backbone Curve Model of Reinforced Concrete Columns Subjected to Cyclic Loading Reversals. *J. Comput. Civil. Eng.* **2018**, *32*, 04018042. [CrossRef]
17. Conforti, A.; Cuenca, E.; Zerbino, R.; Plizzari, G.A. Influence of fiber orientation on the behavior of fiber reinforced concrete slabs. *Struct. Concr.* **2021**, *22*, 1831–1844. [CrossRef]
18. Schmidt, P.; Ungermann, J.; Hegger, J. Contribution of concrete and shear reinforcement to the punching shear resistance of column bases. *Eng. Struct.* **2021**, *245*, 112901. [CrossRef]
19. Shatarat, N.; Salman, D. Investigation of punching shear behavior of flat slabs with different types and arrangements of shear reinforcement. *Case Stud. Constr. Mat.* **2022**, *16*, e01028. [CrossRef]
20. Almahmood, H.; Ashour, A.; Figueira, D.; Yildirim, G. Tests of demountable reinforced concrete slabs. *Structures* **2022**, *46*, 1084–1104. [CrossRef]
21. Liu, X.P.; Bradford, M.A.; Ataei, A. Flexural performance of innovative sustainable composite steel-concrete beams. *Eng. Struct.* **2017**, *130*, 282–296. [CrossRef]
22. Ruiz, M.F.; Muttoni, A. Applications of Critical Shear Crack Theory to Punching of Reinforced Concrete Slabs with Transverse Reinforcement. *ACI. Struct. J.* **2009**, *106*, 485–494.
23. Caldentey, A.P.; Lavaselli, P.P.; Peiretti, H.C.; Fernandez, F.A. Influence of stirrup detailing on punching shear strength of flat slabs. *Eng. Struct.* **2013**, *49*, 855–865. [CrossRef]
24. Trautwein, L.M.; Bittencourt, T.N.; Gomes, R.B.; Della-Bella, J.C. Punching Strength of Flat Slabs with Unbraced Shear Reinforcement. *ACI Struct. J.* **2013**, *108*, 197–205.
25. Eom, T.S.; Kang, S.M.; Choi, T.W.; Park, H.G. Punching Shear Tests of Slabs with High-Strength Continuous Hoop Reinforcement. *ACI. Struct. J.* **2018**, *115*, 1295–1305. [CrossRef]
26. Setiawan, A.; Vollum, R.L.; Macorini, L.; Izzuddin, B.A. Numerical modelling of punching shear failure of reinforced concrete flat slabs with shear reinforcement. *Mag. Concr. Res.* **2021**, *73*, 1205–1224. [CrossRef]
27. Liberati, E.A.P.; Marques, M.G.; Leonel, E.D.; Almeida, L.C.; Trautwein, L.M. Failure analysis of punching in reinforced concrete flat slabs with openings adjacent to the column. *Eng. Struct.* **2019**, *182*, 331–343. [CrossRef]
28. Gosav, A.V.; Kiss, Z.I.; Onet, T.; Bompa, D.V. Failure assessment of flat slab-to-column members. *Mag. Concr. Res.* **2013**, *68*, 887–901. [CrossRef]
29. Lu, X.Z.; Guan, H.; Sun, H.L.; Zheng, Z.; Fei, Y.G.; Yang, Z.; Zuo, L.X. A preliminary analysis and discussion of the condominium building collapse in surfside, Florida, US, June 24. *Front. Struct. Civ. Eng.* **2021**, *15*, 1097–1110. [CrossRef]
30. Mari, A.; Cladera, A.; Oller, E.; Bairan, J.M. A punching shear mechanical model for reinforced concrete flat slabs with and without shear reinforcement. *Eng. Struct.* **2018**, *166*, 413–426. [CrossRef]
31. Jang, J.I.; Kang, S.M. Punching Shear Behavior of Shear Reinforced Slab-Column Connection with Varying Flexural Reinforcement. *Int. J. Concr. Struct.* **2019**, *13*, 29. [CrossRef]
32. Kueres, D.; Schmidt, P. Two-parameter kinematic theory for punching shear in reinforced concrete slabs with shear reinforcement. *Eng. Struct.* **2019**, *181*, 216–232. [CrossRef]
33. de Oliveira, V.H.D.; de Lima, H.J.N.; Melo, G.S. Punching shear resistance of flat slabs with different types of stirrup anchorages such as shear reinforcement. *Eng. Struct.* **2022**, *253*, 113691.
34. Ferreira, M.P.; Pereira, M.J.M.; Freitas, M.V.P.; Neto, A.F.L.; Melo, G.S.S.A. Experimental resistance of slab-column connections with prefabricated truss bars as punching shear reinforcement. *Eng. Struct.* **2021**, *233*, 111903. [CrossRef]
35. Kang, S.M.; Na, S.J.; Hwang, H.J. Punching shear strength of reinforced concrete transfer slab-column connections with shear reinforcement. *Eng. Struct.* **2021**, *243*, 106604. [CrossRef]
36. Vu, D.T.; Hoang, N.D. Punching shear capacity estimation of FRP-reinforced concrete slabs using a hybrid machine learning approach. *Struct. Infrastruct. Eng.* **2016**, *12*, 1153–1161. [CrossRef]
37. Tamimi, M.F.; Alshannaq, A.A.; Qamar, M.I.A. Sensitivity and reliability assessment of buckling restrained braces using machine learning assisted-simulation. *J. Constr. Steel Res.* **2023**, *211*, 108187. [CrossRef]
38. Hu, S.L.; Qiu, C.X.; Zhu, S.Y. Machine learning-driven performance-based seismic design of hybrid self-centering braced frames with SMA braces and viscous dampers. *Smart Mater. Struct.* **2022**, *31*, 105024. [CrossRef]
39. Asgarkhani, N.; Kazemi, F.; Jakubczyk-Galczynska, A.; Mohebi, B.; Jankowski, R. Seismic response and performance prediction of steel buckling-restrained braced frames using machine-learning methods. *Eng. Appl. Artif. Intel.* **2024**, *128*, 107388. [CrossRef]
40. Nguyen, H.D.; Dao, N.D.; Shin, M. Machine learning-based prediction for maximum displacement of seismic isolation systems. *J. Build. Eng.* **2022**, *51*, 104251. [CrossRef]

41. Asgarkhani, N.; Kazemi, F.; Jankowski, R. Machine learning-based prediction of residual drift and seismic risk assessment of steel moment-resisting frames considering soil-structure interaction. *Comput. Struct.* **2023**, *289*, 107181. [CrossRef]
42. Akbarpour, H.; Akbarpour, M. Prediction of punching shear strength of two-way slabs using artificial neural network and adaptive neuro-fuzzy inference system. *Neural Comput. Appl.* **2017**, *28*, 3273–3284. [CrossRef]
43. Tran, V.L.; Kim, S.E. A practical ANN model for predicting the PSS of two-way reinforced concrete slabs. *Eng. Comput.* **2020**, *37*, 2303–2327. [CrossRef]
44. Lee, H.; Lee, H.S.; Suraneni, P. Evaluation of carbonation progress using AIJ model, FEM analysis, and machine learning algorithms. *Const. Build. Mater.* **2020**, *259*, 119703. [CrossRef]
45. Mellios, N.; Uz, O.; Spyridis, P. Data-based modeling of the punching shear capacity of concrete structures. *Eng. Struct.* **2022**, *275*, 115195. [CrossRef]
46. Faridmehr, I.; Nehdi, M.L.; Baghban, M. Novel informational bat-ANN model for predicting punching shear of RC flat slabs without shear reinforcement. *Eng. Struct.* **2022**, *256*, 114030. [CrossRef]
47. Wu, Y.Q.; Zhou, Y.S. Prediction and feature analysis of punching shear strength of two-way reinforced concrete slabs using optimized machine learning algorithm and Shapley additive explanations. *Mech. Adv. Mater. Struct.* **2022**, *30*, 3086–3096. [CrossRef]
48. Shen, Y.X.; Wu, L.F.; Liang, S.X. Explainable machine learning-based model for failure mode identification of RC flat slabs without transverse reinforcement. *Eng. Fail. Anal.* **2022**, *141*, 106647. [CrossRef]
49. Mangalathu, S.; Hwang, S.H.; Jeon, J.S. Failure mode and effects analysis of RC members based on machine-learning-based SHapley Additive exPlanations (SHAP) approach. *Eng. Struct.* **2020**, *219*, 110927. [CrossRef]
50. Zhang, J.G.; Yang, G.C.; Ma, Z.H.; Zhao, G.L.; Song, H.Y. A stacking-CRRL fusion model for predicting the bearing capacity of a steel-reinforced concrete column constrained by carbon fiber-reinforced polymer. *Structures* **2023**, *55*, 1793–1804. [CrossRef]
51. Zhang, D.S.; Lin, X.H.; Dong, Y.L.; Yu, X.H. Machine-Learning-Based uncertainty and sensitivity analysis of Reinforced-Concrete slabs subjected to fire. *Structures* **2023**, *53*, 581–594. [CrossRef]
52. Rahman, J.; Arafin, P.; Billah, A.H.M. Machine learning models for predicting concrete beams shear strength externally bonded with FRP. *Structures* **2023**, *53*, 514–536. [CrossRef]
53. Dong, S.X.; Xie, W.L.; Wei, M.W.; Liu, K.H. Shear design of recycled aggregate concrete beams using a data-driven optimization method. *Structures* **2023**, *55*, 123–137. [CrossRef]
54. Jayasinghe, T.; Chen, B.W.; Zhang, Z.R.; Meng, X.C.; Li, Y.J.; Gunawardena, T.; Mangalathu, S.; Mendis, P. Data-driven shear strength predictions of recycled aggregate concrete beams with/without shear reinforcement by applying machine learning approaches. *Constr. Build. Mater.* **2023**, *387*, 131604. [CrossRef]
55. Ke, G.L.; Meng, Q.; Finley, T.; Wang, T.F.; Chen, W.; Ma, W.D.; Ye, Q.W.; Liu, T.Y. LightGBM: A Highly Efficient Gradient Boosting Decision Tree. *Adv. Neural Inf. Syst.* **2017**, *30*, 3147–3155.
56. Chen, T.; Guestrin, C. XGBoost: A scalable tree boosting system. In Proceedings of the 22nd ACM Sigkdd International Conference on Knowledge Discovery and Data Mining, San Francisco, CA, USA, 13–17 August 2016.
57. Mirjalili, S.; Mirjalili, S.M.; Lewis, A. Grey Wolf Optimizer. *Adv. Eng. Softw.* **2014**, *69*, 46–61. [CrossRef]
58. Meidani, K.; Hemmasian, A.; Mirjalili, S.; Farimani, A.B. Adaptive grey wolf optimizer. *Neural Comput. Abbl.* **2022**, *34*, 7711–7731. [CrossRef]
59. Mirjalili, S.; Lewis, A. The Whale Optimization Algorithm. *Adv. Eng. Softw.* **2016**, *95*, 51–67. [CrossRef]
60. CEB-FIP. *Punching of Structural Concrete Slabs*; CEB-Bull: Lausanne, Switzerland, 2001.
61. Walker, R. Critical Review of EC2 Regarding Punching and Improving the Design Approach. Ph.D. Thesis, Leopold-Franzes-University, Innsbruck, Austria, 2014.
62. Stein, T.; Ghali, A.; Dilger, W. Distinction between punching and flexural failure modes of flat plates. *ACI Struct. J.* **2007**, *104*, 357–365.
63. Rojek, R.; Keller, Y. Slab punching tests with reinforcement with high-strength bond. *Beton-Stahlbetonbau* **2007**, *102*, 548–556. [CrossRef]
64. Ferreira, M.P.; Melo, G.S.; Regan, P.E.; Vollum, R.L. Punching of Reinforced Concrete Flat Slabs with Double-Headed Shear Reinforcement. *ACI Struct. J.* **2014**, *111*, 363–374.
65. Bartolac, M.; Damjanovic, D.; Duvnjak, I. Punching strength of flat slabs with and without shear reinforcement. *Gradevinar* **2015**, *67*, 771–786.
66. Jin, Y.; Yi, W.J.; Hu, L. Experimental study of performance of reinforced concrete slab-column connection with punching shear keys. *Ind. Constr.* **2017**, *47*, 60–65.
67. Dam, T.X.; Wight, J.K.; Parra-Montesinos, G.J. Behavior of Monotonically Loaded Slab-Column Connections Reinforced with Shear Studs. *ACI Struct. J.* **2017**, *114*, 221–232. [CrossRef]
68. Cantone, R.; Ruiz, M.F.; Bujnak, J.; Muttoni, A. Enhancing Punching Strength and Deformation Capacity of Flat Slabs. *ACI Struct. J.* **2019**, *116*, 261–274. [CrossRef]
69. Lewinski, P.M.; Wiech, P.P. Finite element model and test results for punching shear failure of RC slabs. *Arch. Civ. Mech. Eng.* **2020**, *20*, 36. [CrossRef]
70. Jin, Y.; Yi, W.J.; Hu, L.; Ma, K. Experimental analysis on mechanical performances of reinforced concrete two-way slab with studs. *J. Civ. Environ. Eng.* **2019**, *41*, 77–84.

71. Said, M.; Mahmoud, A.A.; Salah, A. Performance of reinforced concrete slabs under punching loads. *Mater. Struct.* **2020**, *53*, 68. [CrossRef]
72. Lima, H.; Palhares, R.; de Melo, G.S.; Oliveira, M. Experimental analysis of punching shear in flat slabs with variation in the anchorage of shear reinforcement. *Struct. Concr.* **2021**, *22*, 1165–1182. [CrossRef]
73. Starosolski, W.; Pajk, Z.; Jansinski, R.; Ukasz, D. Punching shear test of R/C slabs with double headed studs. In Proceedings of the International Scientific Conference on Quality and Reliability in Building Industry; 1999. Available online: https://www.researchgate.net/profile/Jasinski-Radoslaw/publication/317045998_PUNCHING_SHEAR_TEST_OF_RC_SLABS_WITH_DOUBLE_HEADED_STUDS/links/5922f3330f7e9b997945b19b/PUNCHING-SHEAR-TEST-OF-R-C-SLABS-WITH-DOUBLE-HEADED-STUDS.pdf (accessed on 2 April 2024).
74. Taffese, W.Z.; Espinosa-Leal, L. Prediction of chloride resistance level of concrete using machine learning for durability and service life assessment of building structures. *J. Build. Eng.* **2022**, *60*, 105146. [CrossRef]
75. Liang, S.X.; Shen, Y.X.; Ren, X.D. Comparative study of influential factors for punching shear resistance/failure of RC slab-column joints using machine-learning models. *Structures* **2022**, *45*, 1333–1349. [CrossRef]
76. Muttoni, A. Punching shear strength of reinforced concrete slabs without transverse reinforcement. *ACI Struct. J.* **2008**, *105*, 440–450.
77. Sun, B.C.; Cui, W.J.; Liu, G.Y.; Zhou, B.; Zhao, W.J. A hybrid strategy of Auto ML and SHAP for automated and explainable concrete strength prediction. *Case Stud. Constr. Mat.* **2023**, *19*, e02405.
78. Feng, J.P.; Zhang, H.W.; Gao, K.; Liao, Y.C.; Yang, J.; Wu, G. A machine learning and game theory-based approach for predicting creep behavior of recycled aggregate concrete. *Case Stud. Constr. Mat.* **2022**, *17*, e01653. [CrossRef]
79. Amin, M.N.; Khan, S.A.; Khan, K.; Nazar, S.; Arab, A.M.A.; Deifalla, A.F. Promoting the suitability of rice husk ash concrete in the building sector via contemporary machine intelligence techniques. *Case Stud. Constr. Mat.* **2023**, *19*, e02357. [CrossRef]
80. Rizk, E.; Marzouk, H.; Hussein, A. Punching Shear of Thick Plates with and without Shear Reinforcement. *Case Stud. Constr. Mat.* **2011**, *108*, 581–591.
81. Derogar, S.; Ince, C.; Yatbaz, H.Y.; Ever, E. Prediction of punching shear strength of slab-column connections: A comprehensive evaluation of machine learning and deep learning-based approaches. *Mech. Adv. Mater. Struc.* **2024**, *31*, 1272–1290. [CrossRef]
82. Lovrovich, J.S.; Mclean, D.I. Punching shear behavior of slabs with varying span-depth ratios. *ACI Struct. J.* **1990**, *87*, 507–511.